doi:10.1016/S0022-2836(03)00927-6 J. Mol. Biol. (2003) 332, 795–808

JMB

Available online at www.sciencedirect.com

SCIENCE DIRECT®

ELSEVIER

Mixtures of Wild-type and a Pathogenic (E22G) Form of Aβ40 *in Vitro* Accumulate Protofibrils, Including Amyloid Pores

Hilal A. Lashuel[1,2], Dean M. Hartley[1,2], Benjamin M. Petre[3] Joseph S. Wall[4], Martha N. Simon[4], Thomas Walz[1,3] and Peter T. Lansbury Jr[1,2]*

[1]*Harvard Center for Neurodegeneration and Repair 65 Landsdowne St., Cambridge MA 02139, USA*

[2]*Center for Neurologic Diseases Brigham and Women's Hospital and Department of Neurology Harvard Medical School, 65 Landsdowne St., Cambridge MA 02139, USA*

[3]*Department of Cell Biology Harvard Medical School, 240 Longwood Avenue, Boston, MA 02115, USA*

[4]*Department of Biology Brookhaven National Laboratory, Building 463 Upton, NY 11973, USA*

*Corresponding author

Although APP mutations associated with inherited forms of Alzheimer's disease (AD) are relatively rare, detailed studies of these mutations may prove critical for gaining important insights into the mechanism(s) and etiology of AD. Here, we present a detailed biophysical characterization of the structural properties of protofibrils formed by the Arctic variant (E22G) of amyloid-β protein ($A\beta40_{ARC}$) as well as the effect of $A\beta40_{WT}$ on the distribution of the protofibrillar species formed by $A\beta40_{ARC}$ by characterizing biologically relevant mixtures of both proteins that may mimic the situation in the heterozygous patients. These studies revealed that the Arctic mutation accelerates both Aβ oligomerization and fibrillogenesis *in vitro*. In addition, $A\beta40_{ARC}$ was observed to affect both the morphology and the size distribution of Aβ protofibrils. Electron microscopy examination of the protofibrils formed by $A\beta40_{ARC}$ revealed several morphologies, including: (1) relatively compact spherical particles roughly 4–5 nm in diameter; (2) annular pore-like protofibrils; (3) large spherical particles 18–25 nm in diameter; and (4) short filaments with chain-like morphology. Conversion of $A\beta40_{ARC}$ protofibrils to fibrils occurred more rapidly than protofibrils formed in mixed solutions of $A\beta40_{WT}/A\beta40_{ARC}$, suggesting that co-incubation of $A\beta40_{ARC}$ with $A\beta40_{WT}$ leads to kinetic stabilization of $A\beta40_{ARC}$ protofibrils. An increase in the ratio of $A\beta_{WT}/A\beta_{MUT(Arctic)}$, therefore, may result in the accumulation of potential neurotoxic protofibrils and acceleration of disease progression in familial Alzheimer's disease mutation carriers.

Keywords: Alzheimer's disease; amyloid-β protein (Aβ); amyloid pores; protofibrils; Arctic mutation

Introduction

Alzheimer's disease (AD) is a progressive neurodegenerative disease that is characterized by the presence of extracellular amyloid plaques and intraneuronal neurofibrillary tangles in the brain.[1–3] Biochemical analysis of amyloid plaques revealed that a main constituent is fibrillar aggregates of a 39–42 amino acid residue peptide referred to as the amyloid-β protein (Aβ).[4] Several lines of evidence point towards a central role for the process of Aβ fibril formation in the etiology of AD. Transgenic animals overexpressing mutant forms of its precursor, the amyloid precursor protein (APP), develop amyloid plaques comprising fibrillar Aβ.[5] Several pathogenic AD mutations have been shown to affect the processing of APP, resulting in increased levels of Aβ, in particular

Supplementary data associated with this article can be found at doi: 10.1016/S0022-2836(03)00927-6

Abbreviations used: AD, Alzheimer's disease; Arc, Arctic mutant (E22G); WT, wild-type; AU, analytical ultracentrifugation; SVAU, sedimentation velocity analytical ultracentrifugation; EM, electron microscopy; STEM, scanning transmission electron microscopy; SEC, size-exclusion chromatography; FAD, familial Alzheimer's disease; ThT, thioflavin T; TMV, tobacco mosaic virus.

E-mail address of the corresponding author: plansbury@rics.bwh.harvard.edu

the more amyloidogenic variant Aβ42.[6] These data implicate the process of amyloid fibril formation as the cause of disease progression and neurodegeneration in AD.

The molecular mechanism(s) by which fibrillization may cause neurodegeneration in AD and the nature of the toxic species remains controversial.[7] *In vitro* studies have demonstrated clearly that Aβ fibril formation occurs *via* a complex multi-step nucleated polymerization mechanism that involves discrete soluble oligomeric intermediates termed ADDLS[8] or protofibrils, which disappear upon fibril formation.[9–12] Several lines of evidence suggest that Aβ protofibrils are a pathogenic species. First, there is a lack of a clear correlation between the amount of fibrillar Aβ deposits at autopsy and AD severity,[13] whereas a correlation exists between soluble Aβ levels in the brain and early cognitive dysfunction.[14,15] It is noteworthy that in these studies the location of Aβ (intracellular *versus* extracellular), and its aggregation state (monomer, oligomers, or fibrils) have not been well characterized. Second, transgenic animals that overproduce APP exhibit neuronal and behavioral abnormalities before amyloid plaques can be detected.[16,17] Third, non-fibrillar, oligomeric forms of Aβ alter neuronal function and/or cause cell death.[8,18–20] Fourth, in some models, inhibiting fibril formation does not attenuate Aβ-associated toxicity towards cultured neurons.[21,22] Fifth, an autosomal dominant mutation (APPE693G or Aβ (E22G)) with a clinical phenotype similar to that of idiopathic AD was shown to decrease Aβ production *in vivo* and promote protofibril formation *in vitro*.[23]

Most APP mutations associated with early onset familial Alzheimer's disease (FAD) are thought to accelerate AD by modulating the proteolytic processing of APP, which can increase the total concentration of Aβ in the plasma and cerebrospinal fluid and/or produce an increase in the ratio Aβ42/Aβ40.[24,25] However, the Arctic APP mutation (E693G) is an exception; it causes a reduction in Aβ40 and Aβ42 levels in plasma.[23] A reduction in Aβ42 was observed also in conditioned media from cells transfected with APP_{E693G}.[23] With all the evidence mounting in support of the pathogenic protofibril hypothesis,[26] one possible explanation for the toxicity of the Arctic mutation is that it promotes the formation of toxic aggregates, possibly protofibrils.[23] This hypothesis is supported by the increased propensity of the Arctic variant to form protofibrils *in vitro*. Recently, we showed that $Aβ40_{ARC}$ seems to more rapidly form novel annular and pore-like protofibrillar structures ("amyloid pores"), that resemble those formed by bacterial pore-forming toxins.[27] Here, we present detailed biophysical characterizations of protofibrils formed by $Aβ40_{WT}$ and the Arctic variant ($Aβ40_{ARC}$), as well as the biologically relevant mixtures of the two proteins that may model the situation in the heterozygous patients.

Results

The Arctic mutation accelerates Aβ40 fibrillogenesis *in vitro*

Under the conditions described here, $Aβ40_{ARC}$ forms fibrils more rapidly than $Aβ40_{WT}$. Three different established protocols were used to prepare Aβ40 (the DMSO/water/Tris method, the NaOH method[18] and the NaCl/PO_4 method;[23] see Materials and Methods). $Aβ40_{WT}$, and $Aβ40_{ARC}$ (100 μM) were incubated at room temperature without stirring, and fibril formation was monitored by the thioflavin T (ThT) binding assay. ThT

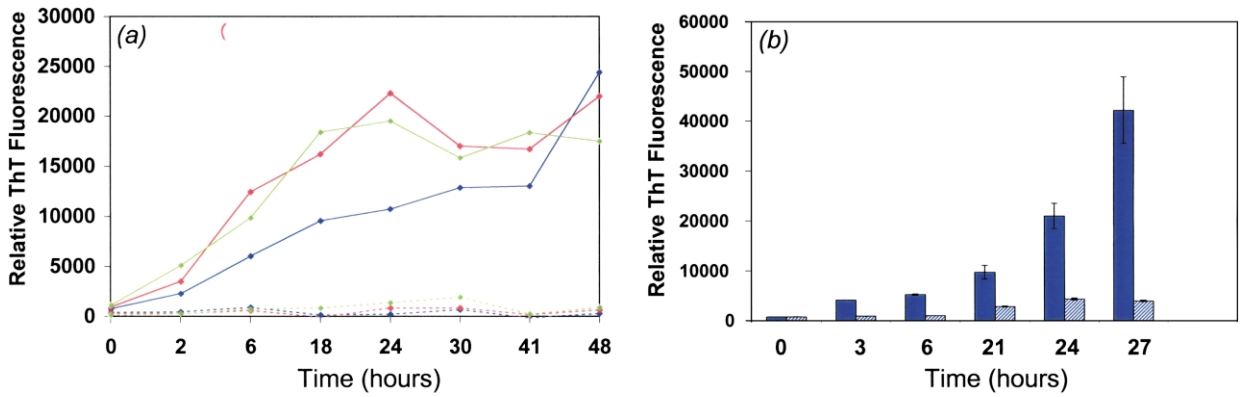

Figure 1. The Arctic mutation accelerates Aβ40 fibrillogenesis. A comparison of amyloid fibril formation (ThT binding) of $Aβ40_{WT}$ (broken lines) and $Aβ40_{ARC}$ (continuous lines) revealed that the Arctic mutation accelerates Aβ fibrillization. (a) Three different protocols (DMSO/water/Tris method, blue; NaOH method, red; and NaCl/PO_4 method, green) were employed to ensure that the aggregation was not dependent on the method of Aβ monomer preparation. $Aβ40_{WT}$ and $Aβ40_{ARC}$ (100 μM) were incubated at room temperature without stirring, and fibril formation was monitored using the ThT binding assay. (b) A fourth method of preparation gave a similar result. In this experiment, $Aβ40_{WT}$ (shaded bars) and $Aβ40_{ARC}$ (filled bars) monomers were isolated by SEC from a GdnHCl-treated A40β stock solution. $Aβ_{WT}$ and $Aβ_{ARC}$ (20 μM) were incubated at 37 °C without stirring, and fibril formation was monitored using the ThT binding assay.

is an amyloid specific dye that exhibits an enhanced emission maximum at 482 nm (excited at 450 nm) upon binding to amyloid fibrils. Fibrillization studies were carried out at room temperature, because the Arctic variant aggregates very rapidly at 37 °C (one to three hours at 100 μM). Figure 1(a) shows that $A\beta40_{ARC}$ showed a gradual increase of the ThT signal during the first 24 hours of incubation, whereas $A\beta40_{WT}$ showed no change in the ThT signal even after 48 hours of incubation (RT) at pH 7.4. The three different protocols yielded similar kinetic profiles for $A\beta40_{WT}$ and $A\beta40_{ARC}$ fibrillogenesis, all consistent with an accelerated rate of fibrillization for $A\beta40_{ARC}$ relative to $A\beta40_{WT}$. To further confirm this finding, we used a fourth preparation protocol; lyophilized $A\beta40_{WT}$ and $A\beta40_{ARC}$ were denatured in 6 M guanidine-HCl (pH 7.4) and loaded onto a Superdex 75 SEC column, producing a single peak corresponding to an unstructured Aβ monomer (as determined by gel-filtration and circular dichroism, data not shown). Monomeric $A\beta40_{ARC}$ and $A\beta40_{WT}$ were collected and subjected to conditions that favor fibril formation (37 °C, pH 7.4) at ~20 μM. Under these conditions, $A\beta40_{ARC}$ fibrillized much faster than $A\beta40_{WT}$ (Figure 1(b)).

The Arctic mutation promotes the formation of annular protofibrils

To probe the effect of the Arctic mutation on the structural properties of Aβ, in particular Aβ protofibrillar intermediates, we monitored the aggregation of $A\beta_{WT}$ and $A\beta_{ARC}$ by electron microscopy

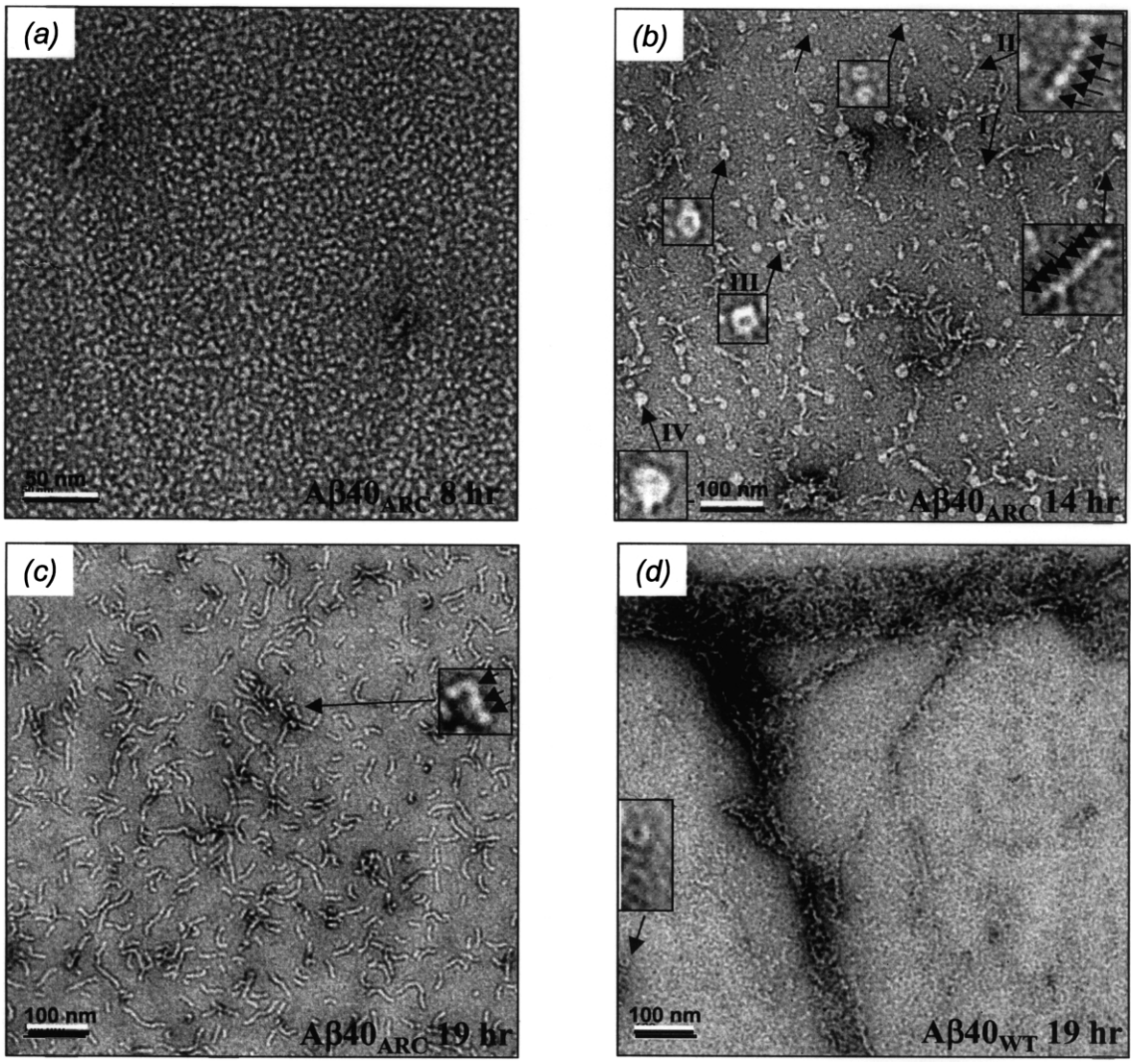

Figure 2. The Arctic mutation promotes the formation of annular protofibrils (amyloid pores). Electron micrograph of negatively stained $A\beta40_{ARC}$ (100 μM) after incubation at room temperature for (a) eight hours, (b) 14 hours and (c) 19 hours. The insets in (b) and (c) show chain-like protofibril (II), whereas (b) (III) and (b) (IV) show annular and globular spheres, respectively. (d) EM image of negatively stained $A\beta40_{WT}$ (100 μM) after incubation at room temperature for 19 hours. The inset demonstrates that annular protofibrils can be formed by $A\beta40_{WT}$, albeit much more slowly and to a lesser extent than the $A\beta40_{ARC}$. Although amyloid fibril formation by $A\beta40_{ARC}$, but not by $A\beta40_{WT}$, was observed during the first 19 hours of incubation, the EM images in this Figure were chosen to focus only on the changes in the structural properties of protofibrillar $A\beta40_{ARC}$.

(EM) as a function of time. $A\beta40_{WT}$ and $A\beta40_{ARC}$ (100 μM) were incubated at room temperature and aliquots were removed at regular intervals and examined by EM. After eight hours, only $A\beta_{ARC}$ showed the formation of predominantly spherical protofibrillar structures with an average diameter of 4.5(±0.5) nm (Figure 2(a)). After 14 hours, spheres (Figure 2(b), I), short chain-like protofibrils (Figure 2(b), II) and annular protofibrils (Figure 2(b), III) were observed for $A\beta40_{ARC}$. The chain-like protofibrils appeared to be composed of ~5 nm spherical species (Figure 2(b), inset). Consistent with earlier reports, the spheres represent the assembly subunit of the chain-like protofibrils.[12,28,29] The annular protofibrils have an outer diameter of 6–9 nm, and an inner diameter of 1.5–2 nm. Large spherical species with an average diameter of 18–24 nm were observed also for $A\beta40_{ARC}$ (Figure 2(b), IV). The amount of spherical and annular protofibrils started to diminish after 19 hours with short filaments and fibrils (not shown in the selected images) emerging as the predominant species, Figure 2(c). Although amyloid fibril formation by $A\beta40_{ARC}$ did occur during the first 19 hours of incubation, the EM images in Figure 2 were chosen to focus only on the changes in the structural properties of protofibrillar $A\beta40_{ARC}$. $A\beta40_{WT}$ (100 μM) did not exhibit significant protofibril formation over the incubation period (at room temperature) of 14–48 hours. However, after 19 hours some non-fibrillar $A\beta40_{WT}$ aggregates and some very rare annular protofibrils could be detected by EM (Figure 2(d)). These observations suggest that the $A\beta40_{WT}$ can form annular pore-like protofibrils, but much more slowly and to a lesser extent than $A\beta40_{ARC}$. Interestingly, after 19 hours the ThT signal for the $A\beta40_{ARC}$ solutions had reached a plateau (Figure 1(a)), and the majority of the monomer was consumed (suggesting complete conversion of $A\beta40_{ARC}$ to fibrils). However, EM showed that a significant amount of $A\beta40_{ARC}$ protofibrils persisted along with amyloid fibrils. Complete conversion of the remaining short chain-like protofibrils to fibrils did occur with time (~72–96 hours). Although we have focused on $A\beta40_{ARC}$, preliminary studies with $A\beta42_{ARC}$ showed annular protofibrils forming more rapidly than $A\beta40_{ARC}$, and annular protofibrils being the predominant protofibrillar species after eight hours of incubation at room temperature (Figure 3).

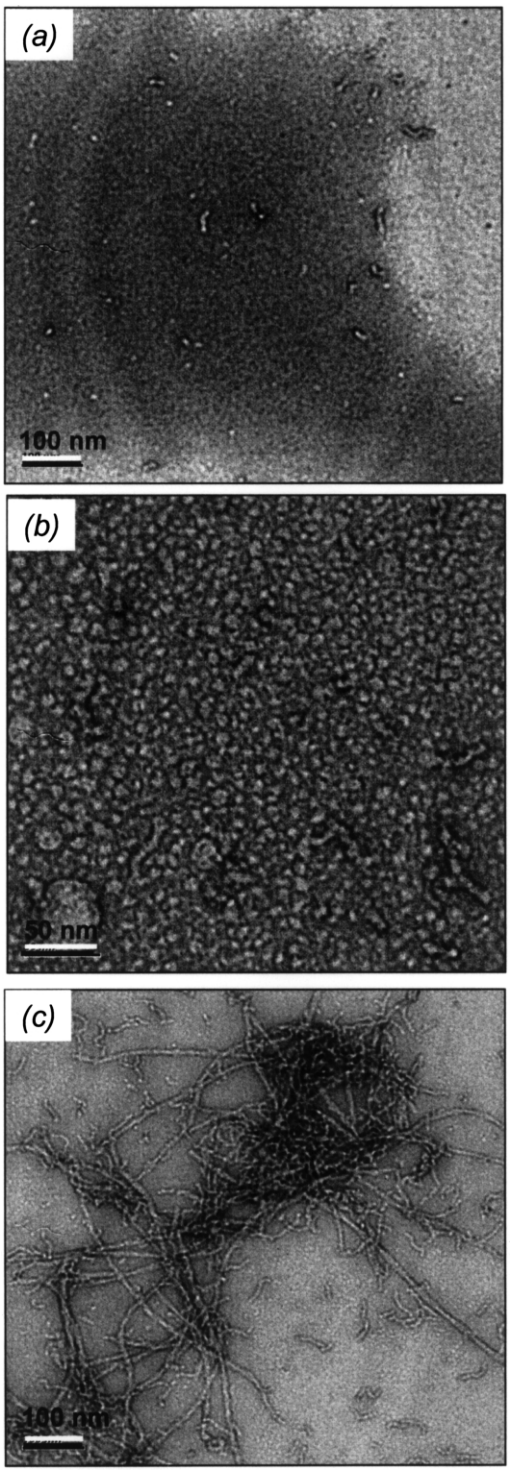

Figure 3. $A\beta42_{ARC}$ forms amyloid pores more rapidly than $A\beta40_{ARC}$. Electron micrograph of negatively stained $A\beta42_{ARC}$ (100 μM) after incubation at room temperature for (a) 30 minutes, (b) eight hours and (c) 19 hours.

Co-incubation of the Arctic variant with $A\beta40_{WT}$ results in the kinetic stabilization of $A\beta40_{ARC}$ protofibrils

AD patients carrying the Arctic mutation are heterozygotes and express both $A\beta_{WT}$ and $A\beta_{ARC}$. However, the ratio of $A\beta_{WT}$ to $A\beta_{ARC}$ ($A\beta = A\beta40 + A\beta42$) in Arctic carriers (equimolar *in vivo* production cannot be assumed) and how it changes with age have not been determined. To determine whether changes in $A\beta40_{ARC}/A\beta40_{WT}$ ratio have an affect on Aβ aggregation *in vitro*, we compared the oligomerization and fibrillization properties of each variant to mixed solutions. During a 70 hour incubation at room temperature, the $A\beta40_{WT}$ (100 μM) sample did not show any significant protofibril formation (not shown) but a small and

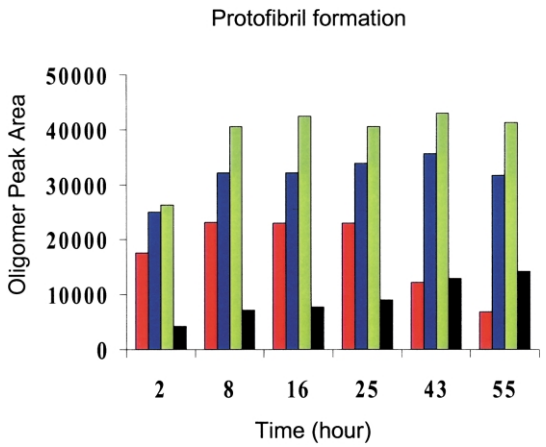

Figure 4. Kinetic stabilization of $A\beta40_{ARC}$ protofibrils by $A\beta40_{WT}$. Protofibril formation during fibrillogenesis was measured using the two Aβ40 variants, $A\beta40_{ARC}$ and $A\beta40_{WT}$ (100 μM), and relevant $A\beta40_{ARC}/A\beta40_{WT}$ mixtures. Red, 100 μM $A\beta40_{ARC}$; blue, 100 μM $A\beta40_{ARC}$/50 μM $A\beta40_{WT}$; green, 100 μM $A\beta40_{ARC}$/100 μM $A\beta40_{WT}$; black, 200 μM $A\beta40_{WT}$.

gradual increase in protofibril formation occurred in the 200 μM $A\beta40_{WT}$ solution (an *in vitro* model of non-carriers "normal") (Figure 4, black). In contrast, $A\beta40_{ARC}$ (≥100 μM) formed protofibril very rapidly. The amount of accumulated $A\beta40_{ARC}$ oligomers remained constant during the first 24 hours (25 °C), but decreased significantly during the next 46 hours (Figure 4, red). This is consistent with the increase in the ThT signal observed at 55 and 70 hours, which coincide with a decrease in the amount of Aβ monomer in solution (see Figure 1 of the Supplementary Material). Interestingly, addition of $A\beta40_{WT}$ (50 or 100 μM) to $A\beta40_{ARC}$ (100 μM) (an *in vitro* model of heterzygous Arctic carriers) resulted in the accumulation of oligomers, which persisted in solution even after 62 hours of incubation (Figure 4, blue and green). These results demonstrate that $A\beta40_{ARC}$ protofibrils (red bars) moved along the assembly pathway more rapidly (43 hours) than protofibrils formed in mixed solutions (blue and green) of $A\beta40_{WT}/A\beta40_{ARC}$, suggesting that addition of $A\beta40_{WT}$ results in the stabilization of $A\beta40_{ARC}$ oligomers.

Fractionation of the protofibril peak results in partial separation of distinct Aβ40 protofibrillar morphologies

EM examination of the protofibrils formed by the Arctic variant revealed several morphologies. To facilitate further characterization of the different protofibrillar species by high-resolution EM and scanning transmission EM (STEM) methods, we sought to partially purify these species by size-exclusion chromatography (SEC) fractionation using the stable protofibrils formed in an equimolar mixture of $A\beta40_{WT}$ (100 μM) and $A\beta40_{ARC}$ (100 μM). After a 16 hour incubation at room temperature, the mixture was spun at 13,000*g*, filtered through a 0.2 μm pore size nylon spin filter (to remove large aggregates) and then separated on a Superose 6 gel-filtration column (4 °C). Aβ40 protofibrils were observed to be stable under these conditions (4 °C, 20–30 hours). The oligomeric Aβ40 eluted as broad peak between the void-volume peak and the Aβ40 monomer peak (Figure 5), suggesting the presence of protofibrils of different sizes and morphologies. The protofibrils were divided into seven fractions, which were concentrated to 15–20 μM and characterized by EM. The EM images (Figure 6) revealed that early fractions (F1–F5, only F2, F4, and F5 are shown) contained predominately short filaments, 4–5 nm wide and 50–100 nm long. Among the filaments were also spherical and ring-shaped structures (~6–9 nm in diameter). In contrast, very few filaments were evident in the late fraction (F7), which contained numerous, ring-shaped structures. In addition, the filaments in fractions F5–F7 were shorter than those in the earlier fractions, suggesting that partial separation of filaments of different sizes was achieved by the Superose 6 column. Examination of fraction F7 revealed that it contained a significant amount of annular protofibrils in addition to the spheres and large spherical oligomeric species. We did observe some variation in protofibril stability between different preparations. In some cases, a shift in the size distribution of the protofibrils toward higher molecular mass protofibrillar species was observed during the 16–24 hour procedure. Shortening both the incubation time for inducing protofibril formation and the fractionation time could minimize these changes. Partial separation of the protofibrillar species was possible; in particular, separation of the chain-like protofibrils from the spheres and annular species. Incubation (20–48 hours) of each of the purified protofibril fractions at 37 °C resulted in their conversion into amyloid fibrils (see Figure 2 of the Supplementary Material), suggesting that they are intermediates on the pathway or are in equilibrium with on-pathway intermediates leading to Aβ fibril formation.

Single-particle averaging reveals a collection of distinct protofibril species

Using a mixed equimolar solution of $A\beta_{ARC}$ and $A\beta_{WT}$ (100 μM each), we employed negative-stain EM and single-particle averaging to analyze fraction F7 (Figure 6) obtained by gel-filtration (Superose 6) fractionation. A representative image of fraction F7 is shown in Figure 7(a). A total of 5126 particles were selected from 25 images of fraction F7. Multi-variate statistical analysis was then used to divide the 5162 particles into 100 output classes. These 100 classes fell into four major groups; the structures are shown in Figure 7(b). The first group consisted of annular structures (amyloid pores) having an average diameter of approximately 6–9 nm and a central stain-filled cavity that is 1.5–2 nm in diameter (Figure 7(b)

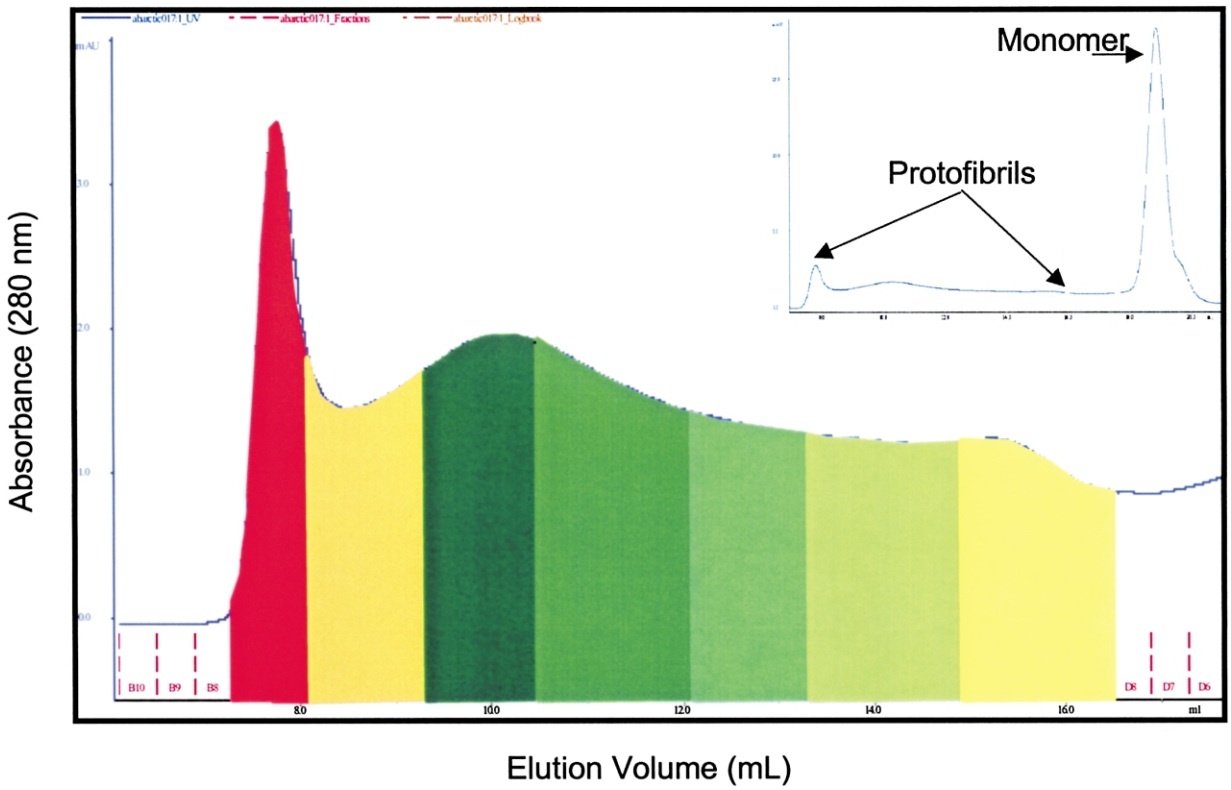

Figure 5. Fractionation of the protofibril peak. Partial separation of Aβ40 protofibrillar species by fractionation of the oligomeric peak on a Superose 6 GF column. Gel-filtration chromatogram illustrating how the Aβ40 oligomeric peak, which was obtained by incubating $A\beta40_{ARC}$ and $A\beta40_{WT}$ at equimolar concentration (100 μM) for 16 hours at room temperature, was divided into seven fractions (F1–F7). The inset shows the amount of protofibrils and monomers present after the 16 hour incubation (RT).

1–3). These amyloid pores are similar to those formed by α-synuclein and reminiscent of those observed for bacterial pore-forming toxins.[27,30,31] The second group showed rectangular particles with a mean diameter of 5 nm and varying length of 12–22 nm (Figure 7(b), 4–6). The third group showed spherical aggregates with a mean diameter of 5(±0.5) nm (Figure 7(b), 7). The fourth group

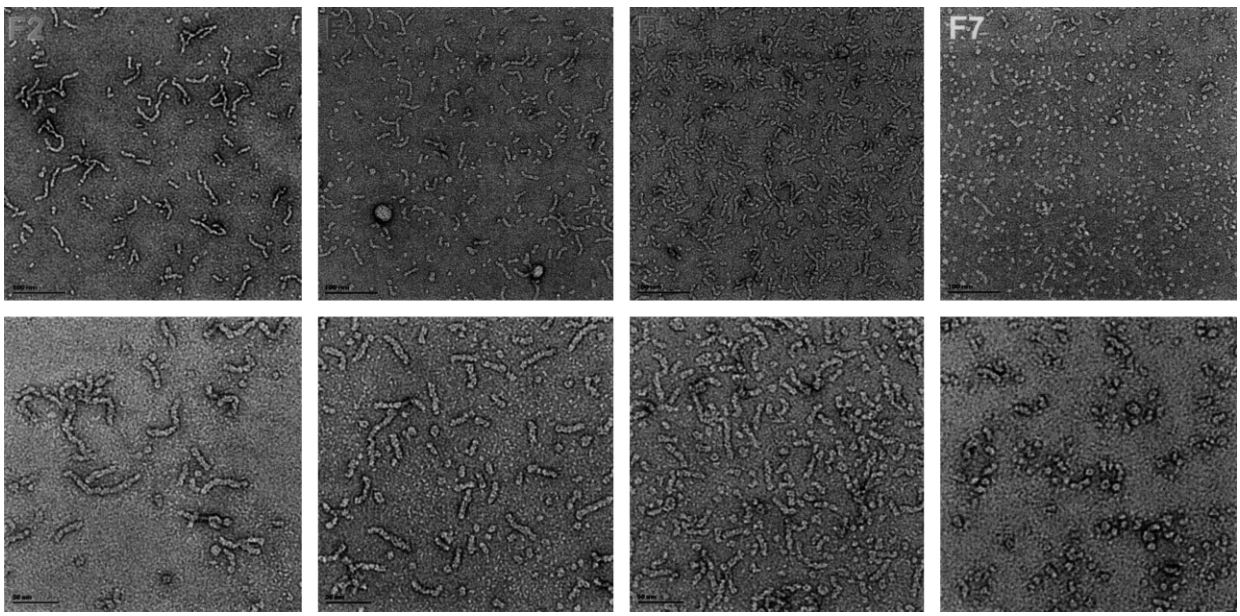

Figure 6. Fractionation of the protofibril peak results in separation of distinct Aβ40 protofibrillar species EM images of fractions F2, F4, F5, and F7 shown at two different magnifications. The scale bars represent 100 nm (top panel) and 50 nm (bottom panel).

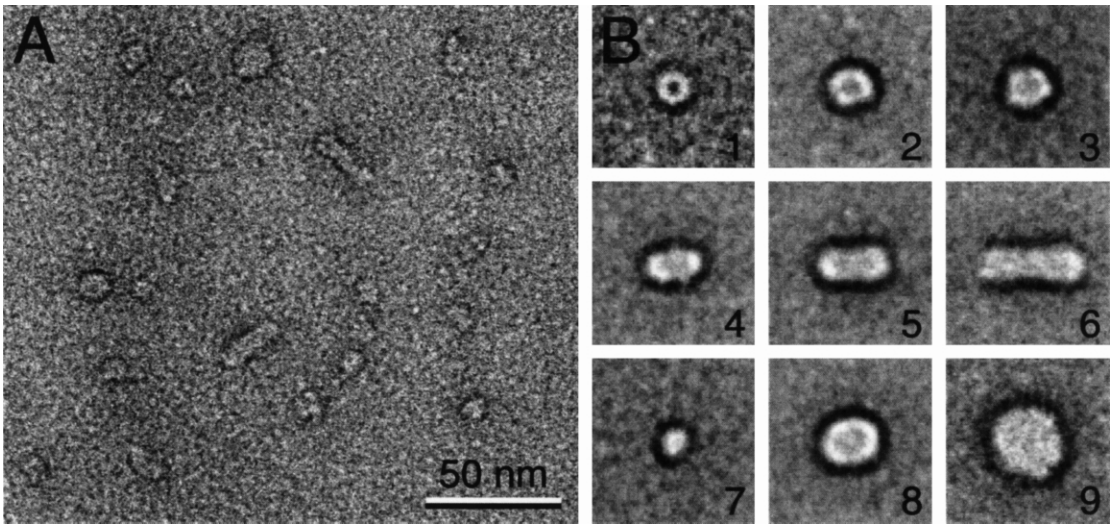

Figure 7. Single-particle averaging reveals a collection of distinct protofibril species. EM image and single-particle averaging of protofibrils reveal pore-like, short filaments and sphere-like morphologies. (a) EM of negatively stained protofibrils from fraction 7 of the Superose 6 GF purified oligomeric peak of an equimolar mixed solution of $A\beta_{ARC}$ and $A\beta_{WT}$ (100 μM), which was incubated for 24 hours at room temperature prior to separation. (b) A gallery of class averages calculated from a total of 5162 particles. The size of each box corresponds to 50 nm.

showed large spherical aggregates, which ranged in diameter from 18 nm to 25 nm (Figure 7(b), 8 and 9). The first, third and fourth groups represent the majority of structures observed in F7.

Quantitative analysis of the molecular mass distribution of Aβ protofibrils by SVAU

To determine the effect of the Arctic mutation on the size distribution of Aβ protofibrils, we performed sedimentation velocity experiments on purified (separated from monomer) protofibrils of $A\beta40_{WT}$, $A\beta40_{ARC}$, $A\beta42_{WT}$, and $A\beta42_{ARC}$. The results, summarized in Table. 1, demonstrate that the Arctic mutation changes the size distribution of Aβ protofibrils in favor of higher molecular mass species, especially in the case of $A\beta42_{ARC}$. In addition, protofibrils formed by $A\beta40_{ARC}$ and $A\beta42_{ARC}$ were observed to undergo rapid conversion towards higher-order protofibrils. For example, sedimentation velocity analytical ultracentrifugation (SVAU) analysis of the total $A\beta_{ARC}$ protofibrils, which were obtained by incubating $A\beta_{ARC}$ (200 μM) for 16–18 hours at room temperature, revealed three populations with average sedimentation coefficients of 8 S, 15 S and 21 S (Figure 8(a)). Further incubation (three to seven hours more) at room temperature resulted in a shift of the sedimentation coefficient distribution towards the 21 S protofibrillar species (Figure 8(b)). In the case of $A\beta42_{ARC}$ conversion into higher-order protofibrils occurred in the analytical ultracentrifuge during sedimentation velocity experiments. This rapid conversion, and the dynamic equilibrium that exist between the different $A\beta_{ARC}$ protofibrillar species and fibrils precluded accurate determination of their molecular mass by sedimentation equilibrium, because 24–30 hours of incubation under centrifugal force are required to reach equilibrium.

Quantitative analysis of the molecular mass distribution of Aβ protofibrils by STEM

STEM can be used to determine the molecular mass of individual particles, independent of their shape or hydrodynamic properties. To estimate the stoichiometric composition of the various Aβ protofibrillar structures (spheres, large spherical structures, annular, and short filaments), the mass distribution of fractions (F5, F6 and F7) rich in these species were analyzed by STEM. Figure 9(a) and (b) shows electron micrographs of unstained/freeze-dried particles obtained from fraction F5 and F7, respectively. A significant number of short filament-like protofibrils were observed in fraction

Table 1. Summary of analytical ultracentrifugation experiments carried out with WT and the Arctic variant of Aβ40 and Aβ42

Peptide	Major species	Minor species	Notes
$A\beta_{WT\ 1-40}$	14 S	32 S	
$A\beta_{ARC\ 1-40}$	15 S	8 S, 21 S	21 S becomes the major species with time at 20 °C.
$A\beta_{WT\ 1-42}$	20 S	29 S	
$A\beta_{ARC\ 1-42}$	90 S, 35 S	26 S	The different species are in dynamic equilibrium

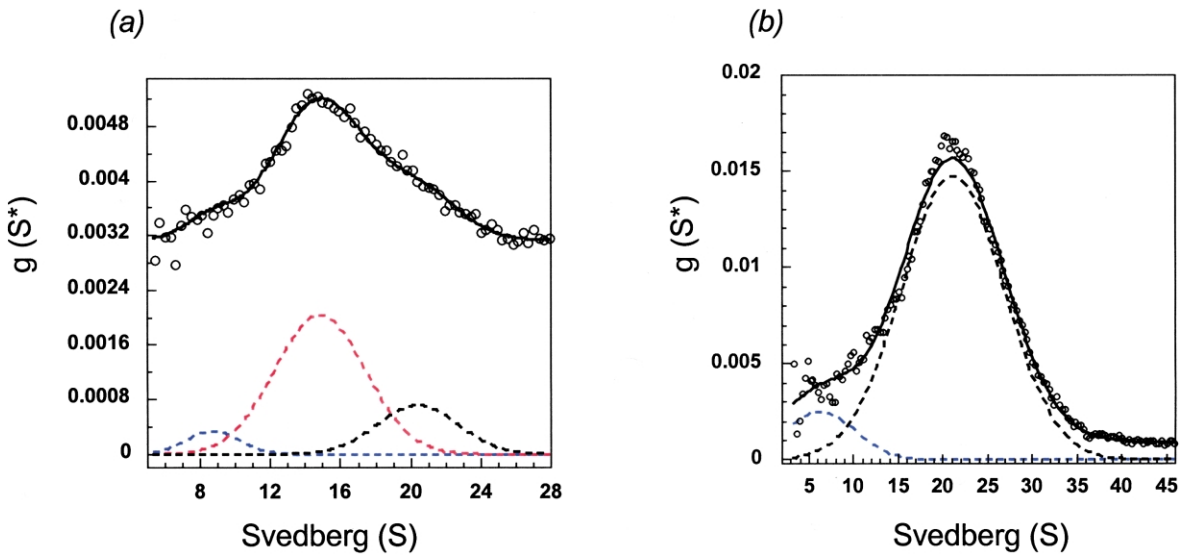

Figure 8. SVAU demonstrates rapid conversion between the different $A\beta40_{ARC}$ protofibrils. The distributions of sedimentation coefficients obtained from experiments performed on purified $A\beta40_{ARC}$ protofibrils. The sedimentation profiles were analyzed using the time-derivative method to yield the apparent distribution of sedimentation coefficients, $g(s^*)$. The prominent maximum corresponds to the sedimentation coefficient of the major species in solution. The black line reflects the best least-squares fit of the data (O) to a three (a) and two species model using a Gaussian function.

F5, whereas spherical protofibrils dominated fraction F7, consistent with the TEM data (Figure 6). Protofibrils of various sizes could be distinguished and selected automatically by using a set of models of overlapping sizes in the PCMass program, which located all isolated particles in each image. The predominant particle shapes observed were: (a) short filaments (F1–F6); (b) relatively amorphous round particles 13–25 nm in diameter (F5–F7); and (c) relatively compact particles roughly 5–8 nm in diameter (F7), occasionally with a central low-density area. Unlike SVAU, where it is difficult to directly assign a specific S value to a particular morphology, in STEM analysis an appropriate model based on the shape of the particles can be chosen to select the particles of each morphology, thus allowing us to estimate the mass distribution of each protofibrillar morphology. In this way, we grouped and analyzed the mass distribution of the short filaments (Figure 9(c)) and spherical species (Figure 9(d)) (spheres of various sizes were grouped together) in the last three fractions (F5, F6 and F7). Global analysis of the short filament-like protofibrils in fractions F5, F6 and F7 (Figure 9(c)) revealed a Gaussian molecular mass distribution with a broad peak of particles ranging in mass from 350 kDa to 800 kDa (81–186 Aβ monomers), with a trailing shoulder at 800–1000 kDa. Analysis of the spherical protofibrils, including annular and large globular structures gave a size from 80–400 kDa, corresponding to 18–93 monomers (Figure 9(d)). The majority of the particles exhibited mass ranging from 150 kDa to 250 kDa (~32–59 monomers). In addition, STEM analysis revealed two other populations with mass distributions ranging from 295 kDa to 450 kDa and 680 kDa to 880 kDa (Figure 8(d)), with the latter species corresponding to the largest spherical aggregates (18–24 nm) observed by EM.

Discussion

The Arctic mutation promotes Aβ oligomerization and fibrillogenesis

Although APP mutations associated with inherited forms of AD are relatively rare, detailed studies of these mutations may prove critical for gaining important insights into the mechanism and etiology of AD.[32] Several mutations (Flemish (A21G), Italian (E22K), Arctic (E22G), Dutch (E22Q) and Iowa (D23N)) that are located around the central hydrophobic core of Aβ accelerate Aβ oligomerization (E22Q,[10] and E22G[23]) and fibrillogenesis (E22Q and D23N[33]). Interestingly, the Flemish mutation was reported to decrease the rate of Aβ fibrillogenesis.[34] The exact mechanism by which these mutations contribute to the pathogenesis of AD is unknown.

While the effect of Aβ mutations on the structure and morphology of Aβ fibrils has been investigated extensively, little is known about the effect of these mutations on the quaternary structure and morphology distribution of early prefibrillar intermediates, the protofibrils. Our studies on the fibrillogenesis of the Arctic variant demonstrate that the Arctic mutation promotes Aβ oligomerization, consistent with data reported by Nilsberth and co-workers.[23] In addition, our data demonstrate that the Arctic mutation accelerates the

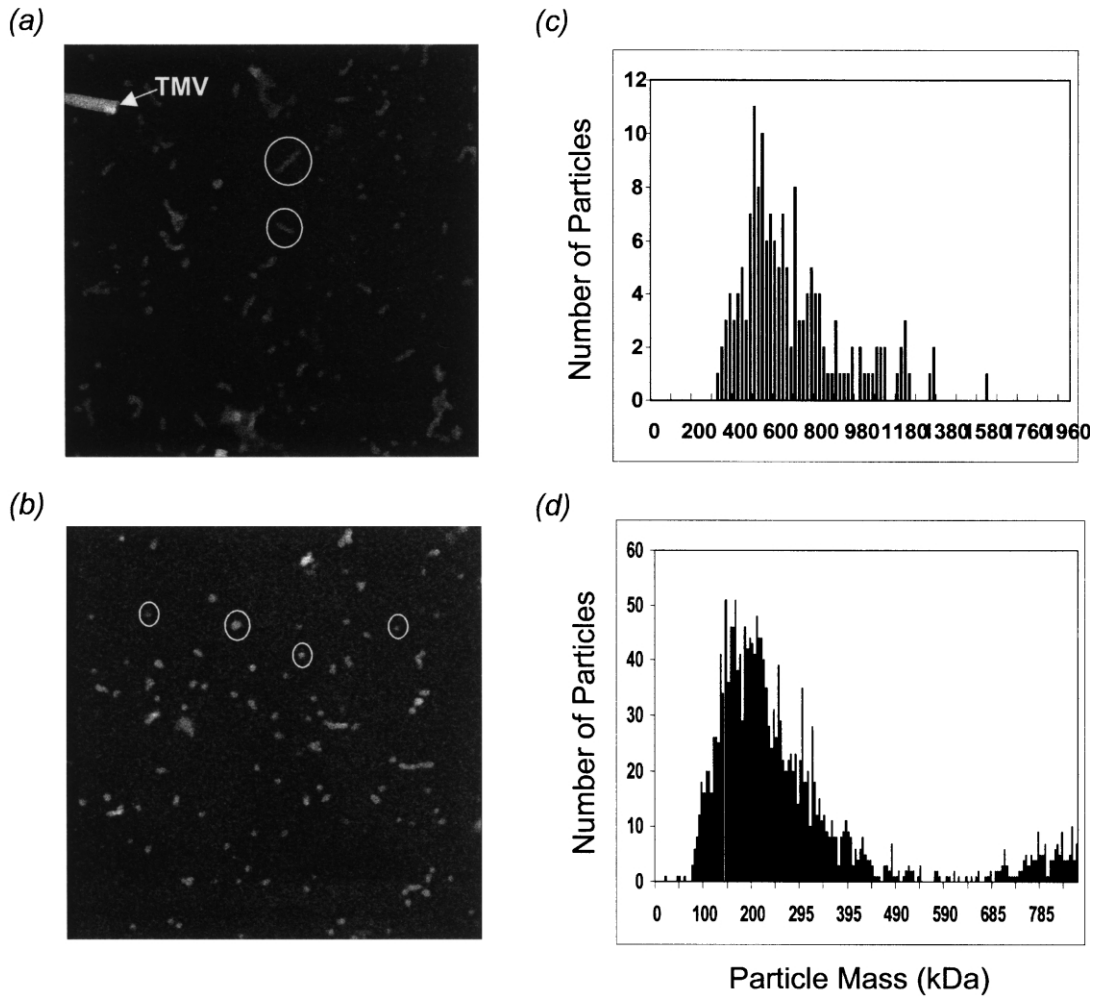

Figure 9. STEM analysis reveals heterogeneous but discrete populations of Aβ40 protofibrils. Quantitative STEM analysis of Aβ40 particles obtained from purified oligomeric fractions of a 1:1 molar ratio solution of $A\beta40_{ARC}$ and $A\beta40_{WT}$ (100 μM). EMs of the unstained/freeze-dried particles of (a) fraction 5 (major species = short filaments) and (b) fraction 7 (major species = spherical and annular structures) and recorded by STEM. Light regions represent areas of high-mass density and dark regions represent areas of low mass density. Tobacco mosaic virus (TMV) was included in each specimen as an internal standard. Histograms showing molecular mass measurements of the particles from oligomeric fraction F5, F6 and F7 using two different models for (c) rectangular and (d) spherical species.

fibrillogenesis of Aβ40. This latter conclusion is in disagreement with data reported by Nilsberth and co-workers,[23] which suggest that this mutation does not affect the rate of Aβ40 fibrillogenesis. The reasons for this disagreement may involve details of experimental conditions. In our studies, the kinetics of Aβ fibril formation was monitored by measuring directly the binding of the amyloid-specific dye ThT to the Aβ fibrils, whereas Nilsberth *et al*. used a technique (SEC) that measures the amount of fibril formation indirectly. Interpretation of the results from the latter approach is likely to be complicated by fibrils dissociation and/or interaction with the column matrix during the SEC experiments. Although the mechanism by which this mutation leads to an acceleration of Aβ oligomerization and fibrillogenesis remains undefined, reduction of the charge state has been proposed to lead to an enhanced rate of oligomerization and/or amyloid fibril formation by amyloid-forming proteins.[35,36]

The different Aβ protofibrillar morphologies seem to be related

Although previous studies have employed SVAU to estimate the molecular size distribution of protofibrils, the heterogeneity of the protofibril preparations used precluded the assignment of molecular mass averages to a particular protofibril species. To address this problem, we characterized our protofibril preparations using STEM, which allows quantitative mass analysis on specific protofibrillar morphologies and sizes. Time-dependent EM studies indicate that the spherical protofibrils (an average diameter of 4.5(±0.5) nm) represent the smallest Aβ protofibrils detectable by EM and STEM. Mass measurements by STEM of the

fraction containing mainly spheres and annular protofibrils (F7), revealed at least three major populations (based on their size) of protofibrils with average masses of 160 kDa, 300 kDa and 800 kDa. The smallest Aβ oligomers (4.5 nm spheres) had an average mass of ~80–100 kDa (19–23 monomers). These results are consistent with earlier reports suggesting that assembly intermediates must contain a minimum of ca 23 Aβ40 monomers.[37] Although fraction F7 contained significant amount of annular protofibrils, it was very difficult to distinguish annular structures from spheres in the unstained STEM images. Based on EM and STEM, we propose that the second protofibrillar population with a mass distribution ranging from 150 kDa to 250 kDa (~32–59 monomers) corresponds to the amyloid pores. The highest mass species (800 kDa) may correspond to the large spherical (18–25 nm) particles observed by EM. The short filaments with chain-like morphology exhibited a wide mass distribution (380–800 kDa), consistent with the observed variability in their length. Given that the 4–5 nm spheres have an average mass of 80–100 kDa, one could conclude that the smallest filament, which has an average mass of 400 kDa, is composed of ~4–5 spherical protofibrillar intermediates. This estimate is consistent with our EM data (Figure 2). The 4–5 nm spherical protofibrils resemble the spherical protofibrils first identified by AFM[9–12] and neurotoxic oligomers referred to as ADDLs.[8] These spheres appear to be the precursors for the short filaments described above (see Figure 2(b), II).[9,12] Additional studies have reported operationally soluble aggregates of Aβ protofibrils with diameters ranging from 8 nm to 18 nm and molecular masses of 0.5 MDa and 1 MDa (based on atomic force microscopy and SVAU measurements).[29,38]

During our studies of Aβ and α-synuclein (both form spherical and annular protofibrils),[27] we have observed that spherical oligomers of both Aβ and α-synuclein seem to have the highest affinity for the mica surface, whereas annular protofibrils have the lowest affinity; very few could be detected using enriched annular fractions (our unpublished results). In contrast, most Aβ protofibrillar species appear to adsorb equally to carbon-coated grids used for EM and STEM studies. These findings underscore the importance of supplementing imaging data (AFM or EM) with data from complementary techniques (SVAU and STEM).

Kinetic stabilization of $A\beta40_{ARC}$ protofibrils by $A\beta40_{WT}$

Individuals with the Arctic form of early onset familial AD are heterozygotes; presumably producing both $A\beta40_{WT}$ and $A\beta40_{ARC}$ in their brains.[23] The ratio of the different Aβ peptides is likely to play a key role in governing the rate of Aβ oligomerization and/or fibrillization, and, possibly, disease progression. Therefore, we compared fibrillogenesis of a mixture of $A\beta40_{WT}$ and $A\beta40_{ARC}$ to the individual variants $A\beta40_{WT}$ and $A\beta40_{ARC}$ (model of a homozygote, none of which is known to exist). Under conditions where $A\beta40_{WT}$ does not produce oligomers or fibrils, $A\beta40_{ARC}$ forms both protofibrils and fibrils. The $A\beta40_{ARC}$ protofibrils formed in the absence of $A\beta40_{WT}$ converted to fibrils, but addition of $A\beta40_{WT}$ to $A\beta40_{ARC}$ resulted in the stabilization and accumulation of protofibrils with eventual conversion to fibrils. The requirement for the relatively high stoichiometry of $A\beta40_{WT}$ (1:1) (addition of 25 μM $A\beta40_{WT}$ to 100 μM $A\beta40_{ARC}$ failed to stabilize protofibrils, data not shown) argues against a simple model where $A\beta40_{WT}$ monomers retard and/or inhibit $A\beta40_{ARC}$ assembly into amyloid fibrils by capping the ends of $A\beta40_{ARC}$ protofibrils. These results suggest that $A\beta40_{WT}$ and $A\beta40_{ARC}$ may interact at an early stage in the aggregation process. Interaction between monomeric $A\beta40_{WT}$ and monomeric and/or protofibrillar $A\beta40_{ARC}$ could interfere with the conformational changes required for protofibril elongation or interfere with protofibril assembly into amyloid fibrils leading to stabilization of $A\beta40_{ARC}$ protofibrils, as has been proposed to explain the inhibitory properties exhibited by Aβ40 against Aβ42 fibril formation.[39] Alternatively, protofibrils formed by $A\beta40_{WT}$ could interact with $A\beta40_{ARC}$ protofibrils in a way that interferes with further $A\beta40_{ARC}$ protofibrils self-assembly into amyloid fibrils. A similar observation has been made for α-synuclein, which is associated with familial Parkinson's disease. Human α-synuclein inhibits amyloid fibril formation of the more amyloidogenic mouse α-synuclein.[40] Further studies are required to distinguish between the models proposed above.

Annular, pore-like protofibrils may be responsible for Aβ permeabilizing or channel-like activity, and possibly AD

While early oligomeric intermediates, protofibrils, have been implicated as the toxic species in several amyloid diseases including PD,[28,30,41–43] HD,[44] British familial dementia,[45] systemic amyloidosis and familial amyloid polyneuropathy,[46–48,8–10] the mechanism of protofibril toxicity is not understood. Recently, we reported that pathogenic mutations in Parkinson's (A53T and A30P) and Alzheimer's disease (Arctic mutation, E22G) promote the formation of a distinct protofibrillar subtype that we refer to as amyloid pores.[27,30] The morphology and the size-selective permeabilization of synthetic vesicles by protofibril fractions containing the annular protofibrils, suggest a pore-like pathogenic mechanism that is reminiscent of bacterial toxins such as α-hemolysin.[49] Furthermore, several amyloid-forming proteins that are associated with neurodegenerative diseases (Alzheimer's disease,

Huntington disease and prion disease) have been demonstrated to form ion-permeable pores *in vitro*, at concentrations that are toxic in cell cultures. In addition, the tendency of amyloid proteins (including Aβ,[27,50] islet amyloid peptide amylin,[51,52] polyglutamine repeats,[53] serum amyloid A,[54] β2-microglobulin,[55] prion proteins[56,57] and α-synuclein[30,58,59]) to form ion-permeable pores correlates with the presence of the pore-like structures. Thus, membrane disruption *via* pore formation may be a general mechanism of cytotoxicity for neurodegenerative diseases.[7,60–62]

In summary, our results suggest that an increase in the ratio of $A\beta_{WT}/A\beta_{ARC}$ in FAD mutation carriers would favor the formation and accumulation of stable protofibrillar intermediates of Aβ, resulting in an enhancement of its neurotoxic properties and accelerated disease progression. Although the nature of the pathogenic species *in vivo* and its mechanism of action remain controversial, our studies suggest that amyloid pore formation and membrane disruption may be linked to the pathogenesis of AD. If this hypothesis is correct, then drug-like molecules that inhibit pore formation and/or membrane permeabilization could be novel therapeutics against AD. Furthermore, the identification of small molecules or mutations that promote or inhibit amyloid pores should facilitate mechanistic studies.

Materials and Methods

Peptides

$A\beta40_{WT}$ and the Arctic variant $A\beta40_{ARC}$ (E22G), were purchased as TFA salts from the Biopolymer Facility at Brigham and Women's Hospital. All peptides were dissolved using their true peptide weight.

Solubilization of Aβ

The WT and Arctic (Arc) peptides were dissolved individually using three different protocols to compare their fibrillogenesis in different buffers: (1) in the DMSO/water/Tris method peptides were dissolved in 100% DMSO then in water and Tris (pH 7.4). The final concentrations of peptide, DMSO, and Tris were 100 μM, 5%, and 10 mM, respectively. (2) The NaOH method,[18] peptides were dissolved using the NaOH method because of its ability to readily dissolve the peptide, control the pH, and reduce the rate of aggregation (see data below). Peptide was dissolved at 4.2 mg/ml in 1 mM NaOH containing phenol red, followed by empirically adding 130–150 μl of 10 mM NaOH to bring the sample to pH 7.0–7.4 using the added phenol red as an indicator. The sample was diluted with water and 10 × PBS, bringing the final peptide concentration to 500 μM in PBS (pH 7.4). Samples were then diluted to 100 μM in water. (3) The $NaCl/PO_4$ method;[23] peptides were dissolved in water to 100 μM, with sodium phosphate and NaCl at final concentrations of 50 mM and 100 mM respectively.

$A\beta40_{WT}$ + $A\beta40_{ARC}$ mixed incubations

Individual peptides were dissolved with NaOH and PBS, as stated above, to give a concentration of 500 μM peptide in PBS (pH 7.4). WT and Arc were combined and diluted in water, giving a final concentration of 100 μM for each peptide.

Preparation and purification of Aβ protofibrils

To prepare Aβ protofibrils, lyophilized synthetic Aβ (WT, Arc, or equimolar mixture of WT and Arc) was dissolved using one of the methods outlined above to obtain a total concentration of 100 μM. The peptide solutions were incubated at room temperature for 16–24 hours, before being centrifuged at 13,000*g* for five minutes to remove any insoluble particle(s). The supernatants were loaded onto either a Superdex 75 HR (Amersham Pharmacia) GF column (used to separate protofibrils from low molecular mass Aβ species) equilibrated with protein buffer (5 mM Tris–HCl (pH 7.4), 70 mM NaCl) or a Superose 6 HR column (used to fractionate Aβ protofibrils) equilibrated with protein buffer (10 mM Tris–HCl (pH 7.4), 150 mM NaCl). The protein was eluted at a flow-rate of 0.5 ml/minute and 0.5 ml fractions were collected. Fractions corresponding to the oligomeric peak were split into seven fractions (F1–F7) and used for biophysical studies. Purified protofibril fractions were stored at 4 °C. Samples for EM and SVAU were prepared and used within one to ten hours unless indicated otherwise.

Quantification of monomeric and oligomeric Aβ by gel-filtration

Samples of Aβ (100 μM), WT, Arc or mixtures of WT and Arc were incubated at room temperature. Aliquots (50 μl) were removed from each sample at various times and filtered through a 0.2 μm pore size nylon spin filter (Costar) to remove any insoluble particle. The filtrate was injected onto a Superdex 200 HR column (10 mm × 30 mm) equilibrated with protein buffer (10 mM Tris–HCl (pH 7.4), 150 mM NaCl). The relative amount of protofibrils and LMW Aβ were quantified by calculating the area under the peak corresponding to each species using the Millenium Software (Waters, Milford, MA).

Thioflavin T assay for fibril formation

Fluorescence measurements of 5 μl of 100 μM Aβ solution in 10 μl of 100 μM ThT + 85 μl of 90 mM glycine–NaOH (pH 8.5 at 25 °C) ($E_x = 450$ nm, $E_m = 482$ nm) as described.[41]

Electron microscopy and image processing

Purified protofibrillar fractions of Aβ were diluted twofold with protein buffer (10 mM Tris–HCl (pH 7.4), 150 mM NaCl) prior to adsorption to glow-discharged, carbon-coated copper grids. Grids were washed with four drops of buffer and stained with two drops of freshly prepared 0.75% (w/v) uranyl formate (Pfaltz & Bauer, Waterbury, CT 06708). Specimens were inspected with a Philips Tecnai 12 electron microscope operated at 120 kV and images were taken at a nominal magnification of 52,000 × using low-dose procedures. For image processing, 25 images of Aβ were digitized with

a Zeiss SCAI scanner using a pixel size of 4.04 Å at the specimen level. From the digitized images, 5162 particles were selected for further computational processing using the SPIDER image processing package.[63] The 5162 particle images were subjected to ten rounds of alignment and classification specifying 100 output classes.

Sedimentation velocity analytical ultracentrifugation (SVAU)

Sedimentation velocity data were collected in a temperature-controlled Beckman XL-A. A double-sector cell, equipped with a 12 mm Epon centerpiece and quartz windows was loaded with 400–420 μl of protein sample. Data were collected at rotor speeds of 3000–60,000 rpm in continuous mode at 25 °C, with a step size of 0.005 cm and an average of three scans per point. Purified void fractions isolated by gel-filtration and stored at 4 °C were incubated at room temperature for one to two hours prior to the SVAU experiments at 25 °C. The sedimentation velocity data were analyzed as described.[30]

Scanning transmission electron microscopy (STEM)

Protofibrillar fractions of Aβ were analyzed by STEM at the Brookhaven National Laboratory using 3–10 μl of the protein samples, as described.[30] Protein samples were applied to a thin carbon film supported by a thick holey film on titanium grids, washed extensively, wicked to a thin layer, frozen rapidly to avoid formation of ice crystals, and freeze-dried overnight. The freeze-dried, unstained specimens were transferred to the STEM under vacuum and examined at −150 °C and 40 kV using the annular dark-field detector mode. Tobacco mosaic virus (TMV) was included in all specimens to monitor preparation quality. Digital images of 512 × 512 pixels with 1 nm spacing were recorded at an average dose of 300–1000 enm^{-2}. The STEM data were analyzed as described, using the PCMass program.[64]

Acknowledgements

We thank Yichin Liu for insightful discussions and for critical review of the manuscript. H.A.L. was a postdoctoral fellow of the Laboratory for Drug Discovery in Neurodegeneration, a core component of the Harvard Center for Neurodegeneration and Repair. Support was derived also from the NIH (AG08470). The molecular EM facility at Harvard Medical School was established by a generous donation from the Giovanni Armenise Harvard Center for Structural Biology and is maintained by funds from NIH grant GM62580. The BNL STEM is an NIH Supported Resource Center, NIH P41-RR01777, with additional support provided by DOE and OBER.

References

1. Selkoe, D. J. (1997). Alzheimer's disease: genotypes, phenotypes, and treatments. *Science*, **275**, 630–631.
2. Castano, E. M. & Frangione, B. (1988). Biology of disease human amyloidosis, Alzheimer disease and related disorders. *Lab. Invest.* **58**, 122–132.
3. Selkoe, D. J. (2000). Toward a comprehensive theory for Alzheimer's disease. Hypothesis: Alzheimer's disease is caused by the cerebral accumulation and cytotoxicity of amyloid beta-protein. *Ann. N.Y. Acad. Sci.* **924**, 17–25.
4. Wang, R., Sweeney, D., Gandy, S. E. & Sisodia, S. S. (1996). The profile of soluble amyloid beta protein in cultured cell media. Detection and quantification of amyloid beta protein and variants by immunoprecipitation-mass spectrometry. *J. Biol. Chem.* **271**, 31894–31902.
5. Janus, C., Phinney, A. L., Chishti, M. A. & Westaway, D. (2001). New developments in animal models of Alzheimer's disease. *Curr. Neurol. Neurosci. Rep.* **1**, 451–457.
6. Lichtenthaler, S. F., Ida, N., Multhaup, G., Masters, C. L. & Beyreuther, K. (1997). Mutations in the transmembrane domain of APP altering gamma-secretase specificity. *Biochemistry*, **36**, 15396–15403.
7. Goldberg, M. S. & Lansbury, P. T., Jr (2000). Is there a cause-and-effect relationship between alpha-synuclein fibrillization and Parkinson's disease? *Nature Cell Biol.* **2**, E115–E119.
8. Lambert, M. P., Barlow, A. K., Chromy, B. A., Edwards, C., Freed, R., Liosatos, M. *et al.* (1998). Diffusible, nonfibrillar ligands derived from Abeta1-42 are potent central nervous system neurotoxins. *Proc. Natl Acad Sci. USA*, **95**, 6448–6453.
9. Harper, J. D., Wong, S. S., Lieber, C. M. & Lansbury, P. T. (1997). Observation of metastable Abeta amyloid protofibrils by atomic force microscopy. *Chem. Biol.* **4**, 119–125.
10. Walsh, D. M., Lomakin, A., Benedek, G. B., Condron, M. M. & Teplow, D. B. (1997). Amyloid beta-protein fibrillogenesis. Detection of a protofibrillar intermediate. *J. Biol. Chem.* **272**, 22364–22372.
11. Walsh, D. M., Hartley, D. M., Kusumoto, Y., Fezoui, Y., Condron, M. M., Lomakin, A. *et al.* (1999). Amyloid beta-protein fibrillogenesis. Structure and biological activity of protofibrillar intermediates. *J. Biol. Chem.* **274**, 25945–25952.
12. Harper, J. D., Wong, S. S., Lieber, C. M. & Lansbury, P. T., Jr (1999). Assembly of A beta amyloid protofibrils: an *in vitro* model for a possible early event in Alzheimer's disease. *Biochemistry*, **38**, 8972–8980.
13. Lemere, C. A., Blusztajn, J. K., Yamaguchi, H., Wisniewski, T., Saido, T. C. & Selkoe, D. J. (1996). Sequence of deposition of heterogeneous amyloid beta-peptides and APO E in Down syndrome: implications for initial events in amyloid plaque formation. *Neurobiol. Dis.* **3**, 16–32.
14. Naslund, J., Haroutunian, V., Mohs, R., Davis, K. L., Davies, P., Greengard, P. & Buxbaum, J. D. (2000). Correlation between elevated levels of amyloid beta-peptide in the brain and cognitive decline. *J. Am. Med. Assoc.*, **283**, 1571–1577.
15. McLean, C. A., Cherny, R. A., Fraser, F. W., Fuller, S. J., Smith, M. J., Beyreuther, K. *et al.* (1999). Soluble pool of Abeta amyloid as a determinant of severity of neurodegeneration in Alzheimer's disease. *Ann. Neurol.* **46**, 860–866.
16. Hsia, A. Y., Masliah, E., McConlogue, L., Yu, G. Q., Tatsuno, G., Hu, K. *et al.* (1999). Plaque-independent disruption of neural circuits in Alzheimer's disease mouse models. *Proc. Natl Acad Sci. USA*, **96**, 3228–3233.
17. Moechars, D., Dewachter, I., Lorent, K., Reverse, D.,

Baekelandt, V., Naidu, A. *et al.* (1999). Early phenotypic changes in transgenic mice that overexpress different mutants of amyloid precursor protein in brain. *J. Biol. Chem.* **274**, 6483–6492.
18. Hartley, D. M., Walsh, D. M., Ye, C. P., Diehl, T., Vasquez, S., Vassilev, P. M. *et al.* (1999). Protofibrillar intermediates of amyloid beta-protein induce acute electrophysiological changes and progressive neurotoxicity in cortical neurons. *J. Neurosci.* **19**, 8876–8884.
19. Bucciantini, M., Giannoni, E., Chiti, F., Baroni, F., Formigli, L., Zurdo, J. *et al.* (2002). Inherent toxicity of aggregates implies a common mechanism for protein misfolding diseases. *Nature*, **416**, 507–511.
20. Walsh, D. M., Klyubin, I., Fadeeva, J. V., Cullen, W. K., Anwyl, R., Wolfe, M. S. *et al.* (2002). Naturally secreted oligomers of amyloid beta protein potently inhibit hippocampal long-term potentiation *in vivo*. *Nature*, **416**, 535–539.
21. Aksenova, M. V., Aksenov, M. Y., Butterfield, D. A. & Carney, J. M. (1996). alpha-1-antichymotrypsin interaction with A beta (1–40) inhibits fibril formation but does not affect the peptide toxicity. *Neurosci. Letters*, **211**, 45–48.
22. Stege, G. J., Renkawek, K., Overkamp, P. S., Verschuure, P., van Rijk, A. F., Reijnen-Aalbers, A. *et al.* (1999). The molecular chaperone alphaB-crystallin enhances amyloid beta neurotoxicity. *Biochem. Biophys. Res. Commun.* **262**, 152–156.
23. Nilsberth, C., Westlind-Danielsson, A., Eckman, C. B., Condron, M. M., Axelman, K., Forsell, C. *et al.* (2001). The "Arctic" APP mutation (E693G) causes Alzheimer's disease by enhanced Abeta protofibril formation. *Nature Neurosci.* **4**, 887–893.
24. Hardy, J. (1997). The Alzheimer family of diseases: many etiologies, one pathogenesis? *Proc. Natl Acad Sci. USA*, **94**, 2095–2097.
25. Lannfelt, L. & Nordstedt, C. (2000). Genetics of Alzheimer's disease—routes to the pathophysiology. *J. Neural. Transm. Suppl.* **59**, 155–161.
26. Haass, C. & Steiner, H. (2001). Protofibrils, the unifying toxic molecule of neurodegenerative disorders? *Nature Neurosci.* **4**, 859–860.
27. Lashuel, H. A., Hartley, D., Petre, B. M., Walz, T. & Lansbury, P. T., Jr (2002). Neurodegenerative disease: amyloid pores from pathogenic mutations. *Nature*, **418**, 291.
28. Ding, T. T., Lee, S. J., Rochet, J. C. & Lansbury, P. T., Jr (2002). Annular alpha-synuclein protofibrils are produced when spherical protofibrils are incubated in solution or bound to brain-derived membranes. *Biochemistry*, **41**, 10209–10217.
29. Huang, T. H., Yang, D. S., Plaskos, N. P., Go, S., Yip, C. M., Fraser, P. E. & Chakrabartty, A. (2000). Structural studies of soluble oligomers of the Alzheimer beta-amyloid peptide. *J. Mol. Biol.* **297**, 73–87.
30. Lashuel, H., Petre, B., Wall, J., Simon, M., Nowak, R., Walz, T. & Lansbury, P. (2002). alpha-Synuclein especially the Parkinson's disease-associated mutants, forms pore-like annular and tubular protofibrils. *J. Mol. Biol.* **322**, 1089–1102.
31. Valeva, A., Schnabel, R., Walev, I., Boukhallouk, F., Bhakdi, S. & Palmer, M. (2001). Membrane insertion of the heptameric staphylococcal alpha-toxin pore. A domino-like structural transition that is allosterically modulated by the target cell membrane. *J. Biol. Chem.* **276**, 14835–14841.
32. Haass, C. & Baumeister, R. (1998). What do we learn from a few familial Alzheimer's disease cases? *J. Neural. Transm. Suppl.* **54**, 137–145.
33. Van Nostrand, W. E., Melchor, J. P., Cho, H. S., Greenberg, S. M. & Rebeck, G. W. (2001). Pathogenic effects of D23N Iowa mutant amyloid beta-protein. *J. Biol. Chem.* **276**, 32860–32866.
34. Walsh, D. M., Hartley, D. M., Condron, M. M., Selkoe, D. J. & Teplow, D. B. (2001). *In vitro* studies of amyloid beta-protein fibril assembly and toxicity provide clues to the aetiology of Flemish variant (Ala692 → Gly) Alzheimer's disease. *Biochem. J.* **355**, 869–877.
35. Chiti, F., Calamai, M., Taddei, N., Stefani, M., Ramponi, G. & Dobson, C. M. (2002). Studies of the aggregation of mutant proteins *in vitro* provide insights into the genetics of amyloid diseases. *Proc. Natl Acad. Sci. USA*, **99**, 16419–16426.
36. Massi, F., Klimov, D., Thirumalai, D. & Straub, J. E. (2002). Charge states rather than propensity for beta-structure determine enhanced fibrillogenesis in wild-type Alzheimer's beta-amyloid peptide compared to E22Q Dutch mutant. *Protein Sci.* **11**, 1639–1647.
37. Kirkitadze, M. D., Condron, M. M. & Teplow, D. B. (2001). Identification and characterization of key kinetic intermediates in amyloid beta-protein fibrillogenesis. *J. Mol. Biol.* **312**, 1103–1119.
38. Snyder, S. W., Ladror, U. S., Wade, W. S., Wang, G. T., Barrett, L. W., Matayoshi, E. D. *et al.* (1994). Amyloid-beta aggregation: selective inhibition of aggregation in mixtures of amyloid with different chain lengths. *Biophys. J.* **67**, 1216–1228.
39. Hasegawa, K., Yamaguchi, I., Omata, S., Gejyo, F. & Naiki, H. (1999). Interaction between A beta(1–42) and A beta(1–40) in Alzheimer's beta-amyloid fibril formation *in vitro*. *Biochemistry*, **38**, 15514–15521.
40. Rochet, J. C., Conway, K. A. & Lansbury, P. T., Jr (2000). Inhibition of fibrillization and accumulation of prefibrillar oligomers in mixtures of human and mouse alpha-synuclein. *Biochemistry*, **39**, 10619–10626.
41. Conway, K. A., Lee, S. J., Rochet, J. C., Ding, T. T., Williamson, R. E. & Lansbury, P. T., Jr (2000). Acceleration of oligomerization, not fibrillization, is a shared property of both alpha-synuclein mutations linked to early-onset Parkinson's disease: implications for pathogenesis and therapy. *Proc. Natl Acad Sci. USA*, **97**, 571–576.
42. Shtilerman, M. D., Ding, T. T. & Lansbury, P. T., Jr (2002). Molecular crowding accelerates fibrillization of alpha-synuclein: could an increase in the cytoplasmic protein concentration induce Parkinson's disease? *Biochemistry*, **41**, 3855–3860.
43. Lee, H. J. & Lee, S. J. (2002). Characterization of cytoplasmic alpha-synuclein aggregates: fibril formation is tightly linked to the inclusion forming process in cells. *J. Biol. Chem.* **277**, 48976–48983.
44. Poirier, M. A., Li, H., Macosko, J., Cai, S., Amzel, M. & Ross, C. A. (2002). Huntingtin spheroids and protofibrils as precursors in polyglutamine fibrilization. *J. Biol. Chem.* **277**, 41032–41037.
45. El-Agnaf, O. M., Nagala, S., Patel, B. P. & Austen, B. M. (2001). Non-fibrillar oligomeric species of the amyloid ABri peptide, implicated in familial British dementia, are more potent at inducing apoptotic cell death than protofibrils or mature fibrils. *J. Mol. Biol.* **310**, 157–168.
46. Lashuel, H. A., Lai, Z. & Kelly, J. W. (1998). Characterization of the transthyretin acid denaturation

pathways by analytical ultracentrifugation: implications for wild-type, V30M, and L55P amyloid fibril formation. *Biochemistry*, **37**, 17851–17864.
47. Lashuel, H. A., Wurth, C., Woo, L. & Kelly, J. W. (1999). The most pathogenic transthyretin variant, L55P, forms amyloid fibrils under acidic conditions and protofilaments under physiological conditions. *Biochemistry*, **38**, 13560–13573.
48. Sousa, M. M., Cardoso, I., Fernandes, R., Guimaraes, A. & Saraiva, M. J. (2001). Deposition of transthyretin in early stages of familial amyloidotic polyneuropathy: evidence for toxicity of nonfibrillar aggregates. *Am. J. Pathol.* **159**, 1993–2000.
49. Wallace, A. J., Stillman, T. J., Atkins, A., Jamieson, S. J., Bullough, P. A., Green, J. & Artymiuk, P. J. (2000). *E. coli* hemolysin E (HlyE, ClyA, SheA): X-ray crystal structure of the toxin and observation of membrane pores by electron microscopy. *Cell*, **100**, 265–276.
50. Hirakura, Y., Lin, M. C. & Kagan, B. L. (1999). Alzheimer amyloid abeta1-42 channels: effects of solvent, pH, and Congo Red. *J. Neurosci. Res.* **57**, 458–466.
51. Anguiano, M., Nowak, R. J. & Lansbury, P. T., Jr (2002). Protofibrillar islet amyloid polypeptide permeabilizes synthetic vesicles by a pore-like mechanism that may be relevant to type II diabetes. *Biochemistry*, **41**, 11338–11343.
52. Mirzabekov, T. A., Lin, M. C. & Kagan, B. L. (1996). Pore formation by the cytotoxic islet amyloid peptide amylin. *J. Biol. Chem.* **271**, 1988–1992.
53. Hirakura, Y., Azimov, R., Azimova, R. & Kagan, B. L. (2000). Polyglutamine-induced ion channels: a possible mechanism for the neurotoxicity of Huntington and other CAG repeat diseases. *J. Neurosci. Res.* **60**, 490–494.
54. Hirakura, Y., Carreras, I., Sipe, J. D. & Kagan, B. L. (2002). Channel formation by serum amyloid A: a potential mechanism for amyloid pathogenesis and host defense. *Amyloid*, **9**, 13–23.
55. Hirakura, Y. & Kagan, B. L. (2001). Pore formation by beta-2-microglobulin: a mechanism for the pathogenesis of dialysis associated amyloidosis. *Amyloid*, **8**, 94–100.
56. Kourie, J. I., Farrelly, P. V. & Henry, C. L. (2001). Channel activity of deamidated isoforms of prion protein fragment 106–126 in planar lipid bilayers. *J. Neurosci. Res.* **66**, 214–220.
57. Kourie, J. I. (2002). Prion channel proteins and their role in vacuolation and neurodegenerative diseases. *Eur. Biophys. J.* **31**, 409–416.
58. Volles, M. J. & Lansbury, P. T., Jr (2002). Vesicle permeabilization by protofibrillar alpha-synuclein is sensitive to Parkinson's disease-linked mutations and occurs by a pore-like mechanism. *Biochemistry*, **41**, 4595–4602.
59. Volles, M. J., Lee, S. J., Rochet, J. C., Shtilerman, M. D., Ding, T. T., Kessler, J. C. & Lansbury, P. T., Jr (2001). Vesicle permeabilization by protofibrillar alpha-synuclein: implications for the pathogenesis and treatment of Parkinson's disease. *Biochemistry*, **40**, 7812–7819.
60. Kagan, B. L., Hirakura, Y., Azimov, R., Azimova, R. & Lin, M. C. (2002). The channel hypothesis of Alzheimer's disease: current status. *Peptides*, **23**, 1311–1315.
61. Lansbury, P. T., Jr & Brice, A. (2002). Genetics of Parkinson's disease and biochemical studies of implicated gene products. *Curr. Opin. Genet. Dev.* **12**, 299–306.
62. Caughey, B. & Lansbury, P. (2003). Protofibrils, pores, fibrils, and neurodegeneration: separating the responsible protein aggregates from their innocent bystandards. *Annu. Rev. Neurosci.* **26**, 267–298.
63. Frank, J., Radermacher, M., Penczek, P., Zhu, J., Li, Y., Ladjadj, M. & Leith, A. (1996). SPIDER and WEB: processing and visualization of images in 3D electron microscopy and related fields. *J. Struct. Biol.* **116**, 190–199.
64. Wall, J. S. & Simon, M. N. (2001). Scanning transmission electron microscopy of DNA–protein complexes. *Methods Mol. Biol.* **148**, 589–601.

Edited by F. E. Cohen

(Received 9 April 2003; received in revised form 26 June 2003; accepted 11 July 2003)

Supplementary Material for this paper comprising two Figures is available on Science Direct